

# The evolution of QSO spectra

Paul J. Francis<sup>1</sup>★ and Anuradha Koratkar<sup>2</sup>★

<sup>1</sup>*School of Physics, University of Melbourne, Parkville, Victoria 3052, Australia*

<sup>2</sup>*Space Telescope Science Institute, 3700 San Martin Drive, Baltimore MD 21218, USA*

Accepted 1994 December 16. Received 1994 November 21; in original form 1994 July 5

## ABSTRACT

We study the rest-frame UV spectra of two samples of QSOs, a low-redshift ( $z \sim 0.4$ ) sample drawn from the *IUE* archives, and a high-redshift ( $z \sim 2.2$ ), optically selected sample, the Large Bright QSO Survey (LBQS). The samples overlap substantially in their range of absolute magnitudes and radio properties, allowing us to study directly the evolution of QSO spectra between redshift  $z \sim 2$  and the present.

We find strong evidence for spectral evolution of QSOs. At *high redshifts only*, we see a new population of radio-quiet QSOs with unusually compact broad-emission-line regions. No significant evolution is seen in the spectra of radio-loud QSOs.

We also find that N v (124.0-nm) emission is weaker in radio-loud QSOs, and that the Baldwin effect is stronger in the red wing of C iv than in the blue.

**Key words:** quasars: emission lines – quasars: general – ultraviolet: galaxies.

## 1 INTRODUCTION

The dramatic decline in the comoving density of bright QSOs between redshift  $z \sim 2$  and the present is well documented, but its cause is not. The present consensus is that the evolution is driven by the rate at which gas is driven into the centres of galaxies (e.g. Small & Blandford 1992; Haehnelt & Rees 1993) by mergers and/or interactions. The evidence is, however, circumstantial, and the postulated link between the kpc-scale merger activity and the sub-pc-scale central engine remains obscure.

Existing studies (e.g. Hamann & Ferland 1992; Baker et al. 1994, in preparation; Delcanton et al. 1994; Osmer, Porter & Green 1994) have not detected any significant spectral evolution, but the limits placed on evolution over the period  $0 < z < 3$  have been loose. In this paper, we combine UV spectra taken with the *IUE* satellite with ground-based spectroscopy of a large, optically selected QSO sample, the Large Bright QSO Survey (LBQS), to study the evolution of the strong rest-frame UV emission lines of QSOs over this redshift range. The *IUE* sample contains many of the brightest known low-redshift QSOs, which have comparable luminosities to the LBQS QSOs, allowing a direct search for evolution uncontaminated by luminosity correlations.

Throughout this paper, we assume  $H_0 = 75 \text{ km s}^{-1} \text{ Mpc}^{-1}$  and  $q_0 = 0.5$ , and magnitudes are  $k$ -corrected using a spectral energy distribution of the form  $F_\nu \propto \nu^{-0.3}$ , where  $F_\nu$  is the

flux per unit frequency and  $\nu$  the frequency. This continuum slope is appropriate for both samples (Neugebauer et al. 1987; Francis et al. 1991), and the results in this paper are insensitive to the exact  $k$ -correction employed.

## 2 SAMPLES

In this section we describe the two samples, with particular emphasis on their differences and biases. Throughout this paper, we will consider the rest-frame wavelength range 117.5–165.0 nm. Only spectra which show the entirety of this wavelength region will be considered. This region includes the strong emission lines of Ly $\alpha$  (121.6 nm), N v (124.0 nm) and C iv (154.9 nm); an increase in the wavelength coverage would seriously reduce the sample sizes. The distribution of the QSOs in redshift and absolute magnitude is shown in Fig. 1.

### 2.1 LBQS

The LBQS consists of 1052 QSOs with apparent photographic  $B_J$ -band magnitudes  $16.0 < M_{B_J} < 18.85$  and redshifts  $0.2 < z < 3.4$ . A description of the survey and plots of the spectra can be found in Foltz et al. (1987, 1989), Chaffee et al. (1991), Hewett et al. (1991) and Morris et al. (1991). LBQS spectra were obtained using the Multiple Mirror Telescope (MMT), whose data provide a spectral coverage of 320–740 nm at 0.6-nm resolution, and with the Du Pont Telescope of the Las Campanas Observatory (LCO, 320–680 nm at 1.0-nm resolution). Each QSO was observed

★ E-mail: pjf@tauon.ph.unimelb.edu.au (PJF); koratkar@stsci.edu (AK).

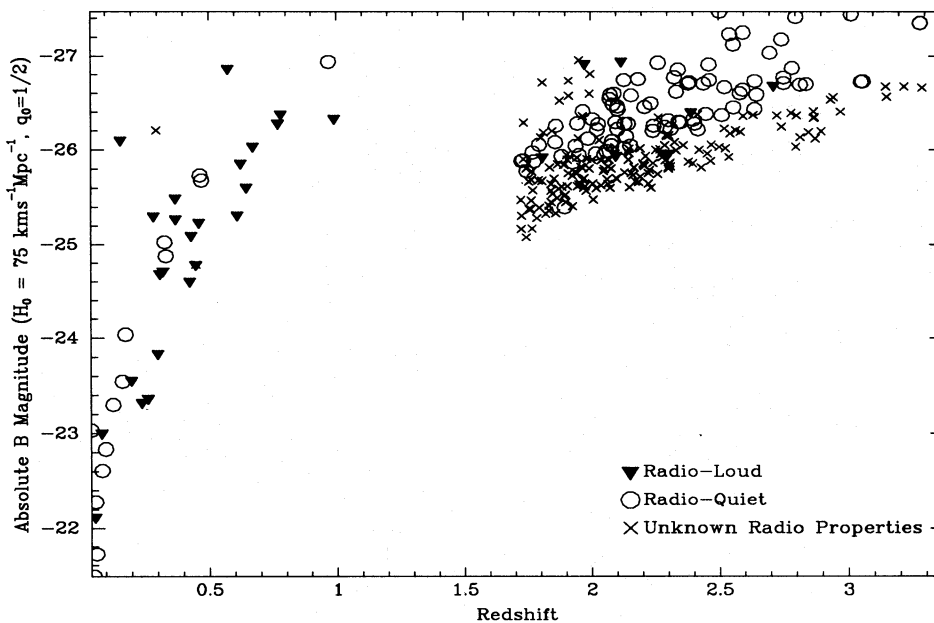


**Figure 1.** Distribution of the two QSO samples in the redshift–absolute magnitude plane. Circles are radio-quiet QSOs, solid triangles radio-loud QSOs, and QSOs without known radio fluxes are plotted as crosses.

until a signal-to-noise ratio of  $\sim 10$  was obtained in the rest-frame wavelength region nearest to 400 nm in the observed frame. Blue magnitudes accurate to 0.15 mag were obtained from machine scans of UK Schmidt direct plates, calibrated by CCD imaging. Redshifts were obtained by cross-correlation against a composite LBQS spectrum (Francis et al. 1991).

LBQS spectra observed with the MMT were taken with a small circular aperture, many at airmasses  $> 1.4$ . As a result, differential atmospheric refraction caused light-loss at the extreme UV ends of some of the spectra (wavelength  $< 400$  nm). This was found to introduce spurious trends in continuum slope against redshift. To minimize this, a composite *observed-frame* spectrum was produced. This was well fitted by a power law multiplied by a differential refraction loss function of unity for wavelengths  $\lambda > 390$  nm, and  $[1.0 + 0.0032(390 - \lambda)]^{-1}$  for  $320 < \lambda < 390$  nm. When all MMT spectra were corrected using this function, the continuum-slope/redshift correlation was greatly reduced (see also Francis 1993b), although the scatter in the continuum slope remains large for the lowest redshift MMT spectra. As we do not consider these observations to be fully spectrophotometric, no analysis of continuum slopes will be attempted in this paper.

Broad-absorption-line QSOs, and other QSOs showing obvious intervening or associated absorption lines, were removed from the sample. Due to the limited signal-to-noise ratio of the spectra, it is likely that weak absorption lines are still present. In particular, no attempt was made to remove Ly $\alpha$  forest absorption, although QSOs with damped Ly $\alpha$  absorbers in the wavelength region of interest were removed. Due to the comparable resolution and mean signal-to-noise ratios of the two samples, any weak residual absorption systems should not bias the comparison.

206 LBQS QSOs show the wavelength range of interest, and lack absorption lines, as discussed in Section 2.4.

## 2.2 IUE sample

The *IUE* sample was drawn from the archives of the *International Ultraviolet Explorer* satellite. All archival spectra of class 85 (quasars) were initially selected. Several of these objects were classified as Seyferts by Véron-Cetty & Véron (1989), and these objects were removed from the sample. The list was checked against the catalogue of Junkkarinen, Hewitt & Burbidge (1991), and all spectra with listed absorption lines removed. Very noisy spectra (mostly high-background spectra) were excluded from the sample.

Spectra were extracted from each of the *IUE* observations using the optimal extraction technique of Kinney, Bohlin & Neill (1991), and we merely summarize the major points. Empirical spline fits were made to the cross-dispersion point-spread function (PSF) along the spectrum, which constrained the PSF to vary smoothly in the dispersion direction. This constraint helps to improve the signal-to-noise ratio of the extracted spectrum relative to the standard IUESIPS, while the flux is still conserved. The flux at each wavelength was then determined by fitting the empirically determined profile, sample by sample, weighted according to the noise model determined from studies of hundreds of other unrelated *IUE* images. Each spectrum was inspected for microphonics pattern, noise spikes and cosmic rays; these were flagged. Errors were associated with each flux value based on the noise model. The extracted net fluxes were converted to absolute fluxes using the *IUE* calibration of Bohlin et al. (1990). A correction was made for the SWP sensitivity degradation (Bohlin & Grillmair 1988, as updated through 1992.5 by Bohlin, private communication). For objects with multiple spectra, the individual spectra were co-added to maximize the signal-to-noise ratio.

*IUE* has a resolution of 0.5 nm at observed-frame wavelengths less than 200 nm, and 0.7 nm at longer wavelengths, roughly a factor of 2 poorer in velocity resolution than the

LBQS. Due to the uncertain positioning of the targets in the spectrograph aperture, the apparent wavelengths of the UV spectra may be in error by  $\sim 0.5$  nm. For this reason, redshifts derived from the UV spectra were used in preference to published redshifts based on the optical spectra. These were measured from the peak of Ly $\alpha$  (121.6 nm), which, as shown below, typically has a strong narrow peak in this sample, permitting a precise redshift determination in even the noisiest spectra.

The mean signal-to-noise ratio of the *IUE* sample is similar to that of the LBQS, but the range is greater. All the measurement techniques discussed in Section 3 were checked to see if there was any systematic dependence of the results on this signal-to-noise ratio classification. No significant dependences were seen, although the scatter of some observations did increase for the lower signal-to-noise ratio spectra.

39 *IUE* QSOs showing the wavelength region of interest and lacking obvious absorption features are used.

### 2.3 Selection effects

The LBQS QSOs are selected from objective prism plates using a variety of criteria. A colour selection criterion is essentially equivalent to the UVX selection method and dominates below redshift 2.2. Above this redshift, Ly $\alpha$  reddens the objective prism spectra, and so selection is dominated by a line-finding criterion. In principle, this may cause slight incompleteness due to the exclusion of particularly weak-lined QSOs. However, no discontinuity is seen in the redshift histogram at  $z=2.2$  (Hewett, Foltz & Chaffee 1993), and no previously known QSO within the LBQS fields and magnitude limits with  $z > 1$  has been missed. As the LBQS is selected in the rest-frame UV, it will be strongly biased toward QSOs with hard UV–optical continua (Francis 1993b; Webster et al. 1995).

The *IUE* sample was drawn from the literature, and does not follow any well-defined selection criteria. Most of the objects were selected because they were the favourite QSOs of the original proposer. We have attempted to find papers describing the original motivations for the *IUE* observations; all published motivations were simply that the QSOs lay in a particular redshift range and were bright enough to be observed with *IUE*, but no reason for the choice was given for about 60 per cent of the spectra. 15 of the QSOs were originally selected by UVX methods, 18 in radio surveys (mainly 3C and Parkes), one by variability, two in the X-rays and three in blue galaxy catalogues. None of the spectra for which we have information were selected because of their spectral properties.

We have to reject the poorest quality spectra to do any meaningful analysis, but this introduces a potential bias. The best spectra will, in general, be those of objects observed many times. This may well be a biased subset, containing, for example, QSOs selected for variability mapping, which might be preferentially chosen to have strong emission lines. To prevent this bias, the decision to reject spectra because of their signal-to-noise ratios was made on the basis of individual spectra, not of co-adds of many spectra. Only 3 per cent of the QSOs in our sample have been observed 10 or more times, so we do not consider this bias to be significant.

A large proportion of our QSOs are drawn from the PG sample (Schmidt & Green 1983). Indeed, 11 of the 13 PG QSOs with  $z > 0.37$  and *B* magnitudes brighter than 16.15 are included in the sample. The other two were observed with *IUE*, but the archive spectra were too poor to be used; all that could be measured was a rough velocity width of one line in each, and these velocity widths were both well within one standard deviation of the sample mean. We thus consider the remaining 11 PG QSOs to be an effectively complete and unbiased subsample. This subsample has UV spectral properties indistinguishable from the rest of the *IUE* sample, so we do not consider the *IUE* sample to be badly biased by its eclectic selection.

### 2.4 Radio

Radio observations have been made for approximately a quarter of the LBQS QSOs (Visnovsky et al. 1992; Hooper et al. 1994, in preparation). Of those observed, roughly 10 per cent were radio-loud, as defined by Francis, Hooper & Impey (1993, hereafter FHI). We use their radio-loudness classification.

All radio-selected *IUE* QSOs are taken to be radio-loud. Given that most of these objects were selected in surveys (such as 3C and the Parkes 2.7-GHz survey) with very high radio flux limits, this assumption is likely to hold for even the least luminous objects. For the PG sample, we used the radio-loudness criterion of Kellerman et al. (1989) to classify QSOs as radio-loud or radio-quiet. This classification is consistent with that used for the LBQS. The only QSOs for which we were unable to find published radio observations were the two X-ray selected ones; they are not found in any published radio catalogues and are therefore either radio-quiet or at the quiet end of the radio-loud population. The analyses below were repeated classifying them as radio-quiet or unknown; no difference was seen in any of the conclusions.

Given the heterogeneous nature of the radio observations of the non-PG *IUE* QSOs, it is possible that a small number may have been misclassified. This does not, however, affect the conclusions of this paper, as the spectral properties of radio-loud and radio-quiet QSOs in the *IUE* sample are very similar (Section 3).

### 2.5 Extended emission

The *IUE* spectra were taken through a  $10 \times 20$  arcsec<sup>2</sup> aperture, corresponding to physical scales of about 20 kpc at  $z \sim 0.05$  up to about 100 kpc for  $z \sim 1$ . The LBQS apertures ( $\sim 2.5$  arcsec) correspond to physical scales of about 15–20 kpc. Thus if there was substantial emission coming from tens of kpc from the nucleus, it would be seen in *IUE* spectra of QSOs with  $z > 0.1$  but not in the LBQS spectra.

At  $z \sim 2$ , extended Ly $\alpha$  emission has been seen on 100-kpc scales around several radio-loud QSOs (Heckman et al. 1991; Hu et al. 1991). It contributes about 10 per cent of the flux of the nuclear Ly $\alpha$  line. The presence of extended Ly $\alpha$  emission around low-redshift QSOs is unknown, but many of the *IUE* sample QSOs have detections or upper limits on their extended [O III] (500.7-nm) emission (Stockton & McKenty 1987; Durret 1989, and references therein). Converting these into Ly $\alpha$  equivalent widths using the upper limits on

the narrow-line region (NLR) line ratios from Wills et al. (1993a), we find that the extended flux contributes <1 per cent of the Ly $\alpha$  from the spatially unresolved core. If we assume that the gas emitting the extended flux is less dense than the NLR, we can increase the extended Ly $\alpha$  emission, at the expense of eliminating extended C IV emission.

We conclude that for radio-loud QSOs in the *IUE* sample with  $z > 0.1$ , the extended emission may contribute up to  $\sim 10$  per cent of the Ly $\alpha$  emission. It is unlikely that the extended emission contributes measurably to the C IV emission or affects the radio-quiet QSOs.

Note that the emission-line component differing between the two samples (Section 3) is spectrally resolved; its velocity width (FWHM) of  $\sim 2500$  km s $^{-1}$  is substantially larger than the instrumental resolution of the *IUE* spectra ( $\sim 1100$  km s $^{-1}$ ). Thus if extended emission was responsible for the inter-sample differences, we require that the gas on 100-kpc scales around the nucleus be travelling with speeds of  $> 2000$  km s $^{-1}$ .

### 3 RESULTS

Due to the notorious subjectivity of measurements of the heavily-blended emission lines of QSOs, we compare the LBQS and *IUE* samples in three different ways: using composite spectra, profile-fitting, and Principal Components Analysis (PCA).

#### 3.1 Composite spectra

All composites are formed by the following steps. (1) Each spectrum is shifted to its rest-frame, and rebinned (conserving flux) into 0.3-nm bins over the wavelength range 117.5–165.0 nm. (2) Each spectrum is scaled such that the mean flux in its wavelength bins over this wavelength range is unity. (3) A composite is formed by averaging the fluxes of all

the different spectra in each bin. No weighting is applied, to avoid signal-to-noise ratio biases.

Care should be taken when looking at the composite spectra, as the summing of spectra with lines of different widths and profiles can in theory produce a mean spectrum bearing little resemblance to any of the individual spectra making it up. Despite this, we believe that the simplicity and model independence of composite spectra make them a useful starting point in this analysis.

In this section we concentrate on qualitative differences; we defer an assessment of the formal confidence of the results to subsequent sections.

##### 3.1.1 Evolution

To test for spectral evolution, we would like to compare mean spectra of samples of the same luminosities but different redshifts. If we take the brighter half of the *IUE* sample (absolute magnitude  $< -24.8$ ), this subsample has a mean absolute magnitude of  $-25.8$ , very close to that of the LBQS,  $-26.1$ . The composite spectra of this bright *IUE* subsample and of the LBQS are compared in Fig. 2.

A number of differences are seen. At wavelengths shorter than Ly $\alpha$ , the *IUE* composite lies above the LBQS composite, as would be expected from the integrated effect of Ly $\alpha$  forest absorption lines. C IV and Ly $\alpha$  are stronger in the *IUE* subsample, with the largest differences at the cores of the lines. N V is weaker in the *IUE* subsample. He II (164.0 nm) is possibly stronger in the *IUE* sample.

As a check on these results, and to test if the differences still appear in less luminous QSOs, we use the composite spectrum of Boyle (1990). This is derived from a UVX-selected sample of about 400 QSOs, and the spectra which make up its UV end (used here) have a mean absolute magnitude of  $-24.3$ , close to the mean absolute magnitude of the whole *IUE* sample,  $-24.6$ . The Boyle composite spectrum

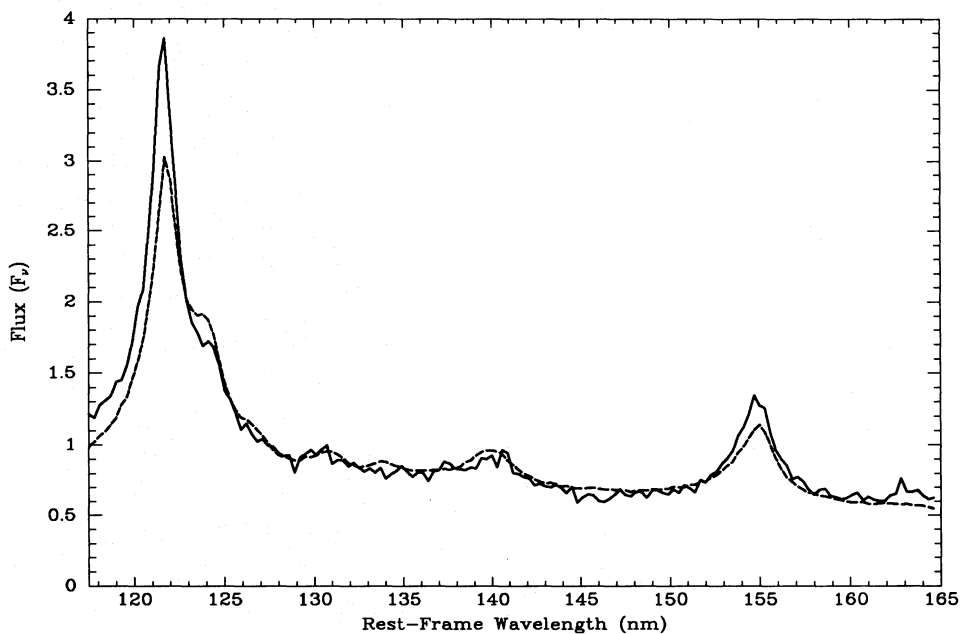


Figure 2. Composite spectra of the LBQS sample (dashed line) and of the bright *IUE* subsample (solid line).

and the composite spectrum of the entire *IUE* sample are compared in Fig. 3. The spectra making up the Boyle composite were not flux-calibrated, and so to make the composite, a low-order polynomial fit was divided into each. To aid comparison, we have multiplied the Boyle composite by a power law chosen to make it match the continuum shape of the LBQS composite.

Once again, the *IUE* sample has stronger emission at the cores of Ly $\alpha$  and C IV, and weaker N v emission. No difference is seen in the Ly $\alpha$  forest; we ascribe this to the polynomial fitting used in the construction of the Boyle composite, which will tend to take out changes in the continuum level.

We conclude that the *IUE* sample spectra have, on average, stronger cores to their Ly $\alpha$  and C IV emission, and weaker N v emission, as compared to higher redshift, optically selected QSOs with the same absolute magnitude.

### 3.1.2 Radio properties

The mean UV spectra of radio-loud and radio-quiet QSOs in the LBQS have been compared by FHI. They found marginally significant differences; the cores of Ly $\alpha$  and C IV were stronger in the radio-loud QSOs. The differences they found between radio-loud and radio-quiet QSOs strongly resemble the differences found above between the *IUE* and LBQS samples.

In Fig. 4, we compare the composite spectra of the radio-loud and radio-quiet QSOs of the *IUE* sample. Unlike the two FHI composites, the spectra of the radio-loud and radio-quiet QSOs in the *IUE* sample are very similar.

The *IUE* sample is 59 per cent radio-loud, while the LBQS is only  $\sim 10$  per cent radio-loud (Visnovsky et al. 1992). Could this be responsible for the differences between their composite spectra? The similarity of the radio-loud and radio-quiet *IUE* spectra suggests not. Even if we construct an

artificial LBQS composite by adding the radio-loud and radio-quiet LBQS composites, weighted as if the LBQS had the same fraction of radio-loud QSOs as the *IUE* sample, it still cannot account for more than half the difference.

We conclude that the different radio-loud fractions of the low- and high-redshift samples probably cannot explain all the observed differences in the line cores. Indeed, there seems to be evolution in the difference between radio-loud and radio-quiet QSOs.

The one large difference between the spectra of radio-loud and radio-quiet QSOs seen in the *IUE* sample (Fig. 4) is the relative weakness of N v emission in the radio-loud QSOs. This was also seen by FHI, and is noted by Osmer, Porter & Green (1994). We do not attempt to measure this from the composites, given the difficulty of deblending Ly $\alpha$  and N v, but qualitatively it appears sufficient to explain the small N v differences seen between the high- and low-redshift samples.

### 3.1.3 Baldwin effect

Our samples, when combined with the Boyle composite, span an order of magnitude in luminosity both at redshift  $z \sim 2$  and low redshift. This provides an opportunity to measure the Baldwin effect (the well-established anticorrelation of equivalent widths and luminosity) directly, without correction for QSO evolution.

At  $z \sim 2$ , the QSOs making up the UV end of the Boyle composite are a factor of 5 less luminous than those making up the LBQS composite, and as both are at the same redshift, this factor is cosmology-independent. The two composite spectra are compared in Fig. 5.

We obtain a quantitative estimate of the strength of the Baldwin effect as follows. A power-law continuum is subtracted from the two composite spectra. This is done twice, choosing continua as different as seems plausible, to assess

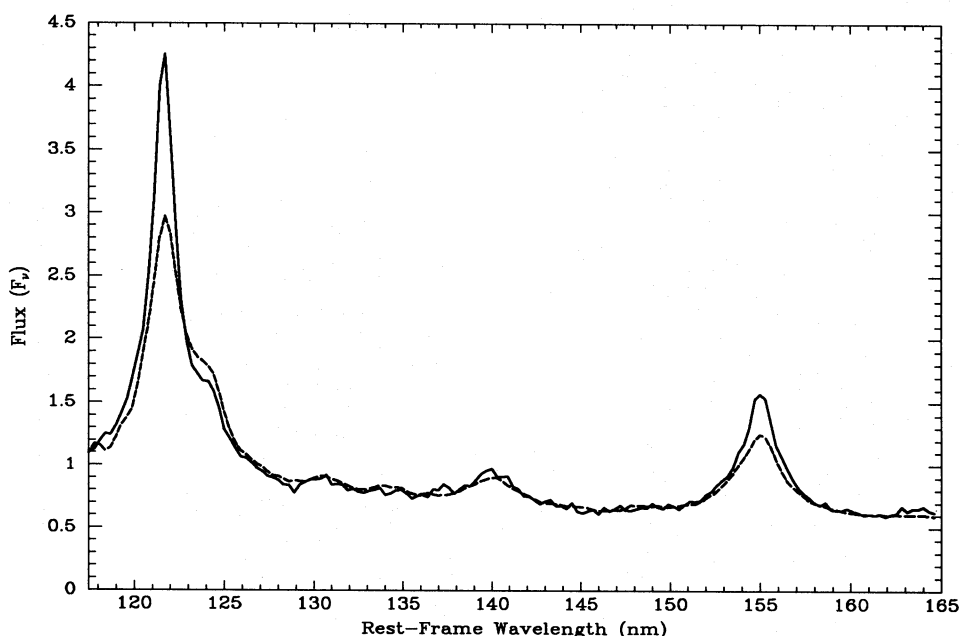


Figure 3. Composite spectrum of the *IUE* sample (solid line) compared with the composite spectrum from Boyle et al. (1990) (dashed line).

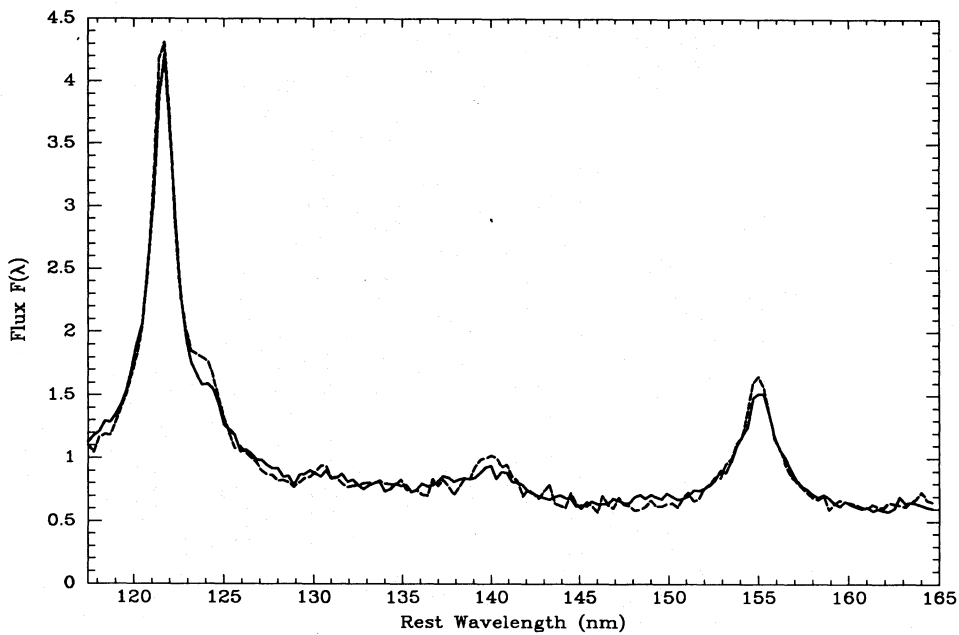


Figure 4. Composite spectra of the radio-loud (solid line) and radio-quiet (dashed line) IUE QSOs.

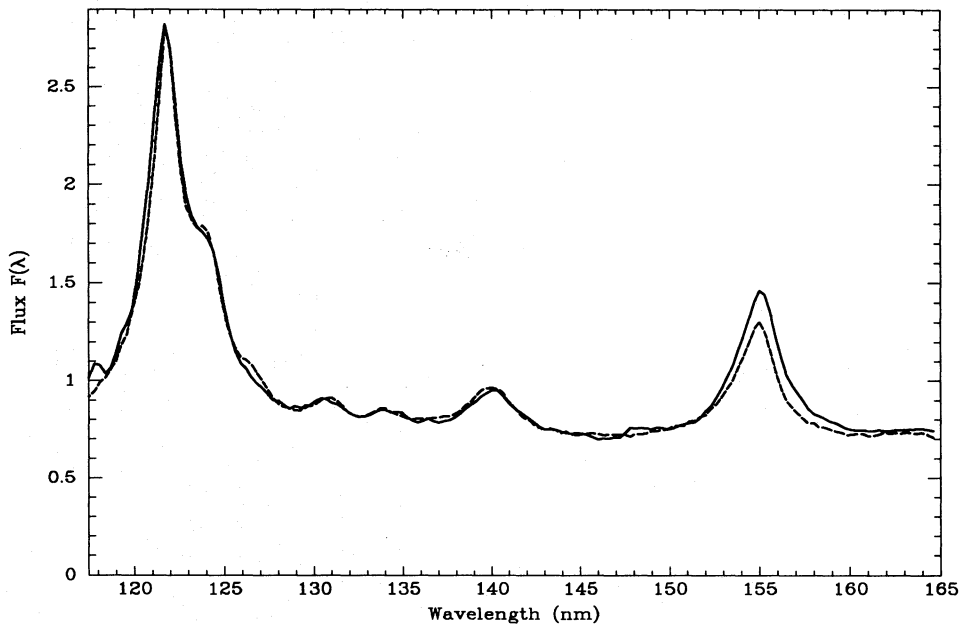
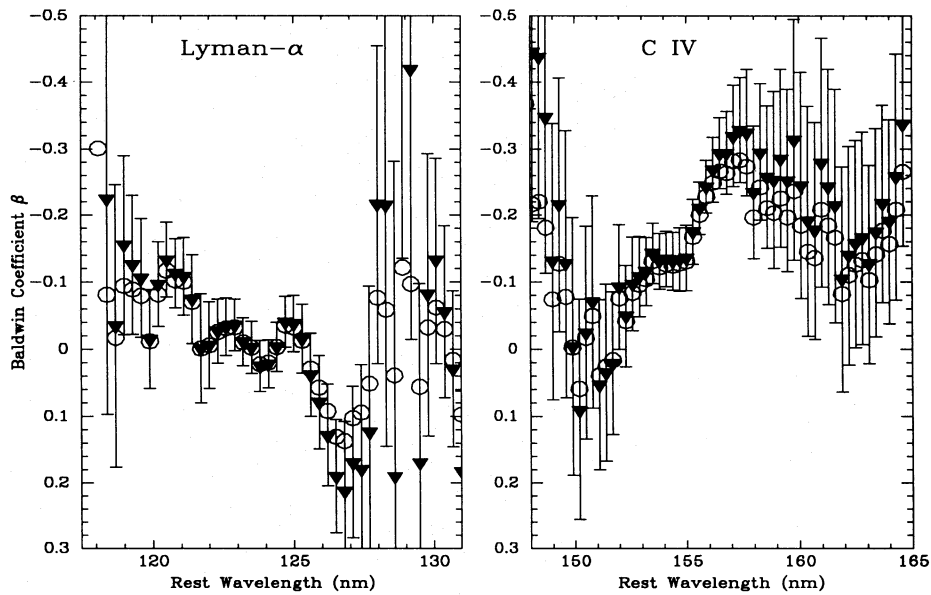


Figure 5. Composite spectra of the LBQS (dashed line) compared with composite spectrum of Boyle (1990).

the errors this procedure introduces. The continuum-subtracted composite spectra are ratioed, and the ratio spectrum converted into a spectrum of the wavelength dependence of the Baldwin index  $\beta$ , where the equivalent width at a particular wavelength  $\lambda$  is  $W_\lambda \propto L^\beta$ , and  $L$  is the QSO luminosity in the rest-frame  $B$  band. Errors are measured by constructing a standard-deviation spectrum (Francis et al. 1991) whose bins are the standard deviations of the fluxes of all the spectra comprising the composite. The standard deviations are divided by the square root of the number of spectra making up each composite, and then

propagated through the analysis. The errors will have contributions from the Poisson noise in the individual spectra, but in practice the uncertainty in each mean spectrum, and hence in the measurements of the Baldwin effect, is dominated by the spectrum-to-spectrum diversity in line strengths. For this reason, resultant errors will strongly correlate. As no standard-deviation spectrum is available for the Boyle sample, the LBQS standard-deviation spectrum was used. The quantitative measurements of the Baldwin index are shown in Fig. 6; values using both continuum fits are plotted.



**Figure 6.** Wavelength dependence of the Baldwin effect, from the comparison of the Boyle and LBQS composite spectra. Solid triangles and error bars are derived from a best 'by eye' power-law continuum fit, while circles are derived from an alternative continuum fit, as described in the text.

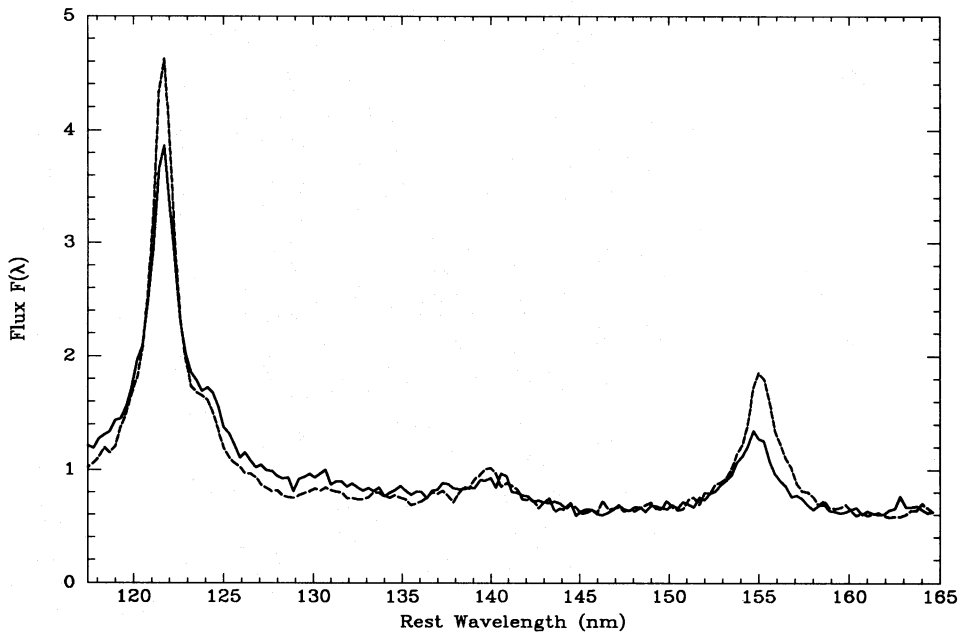


**Figure 7.** Composite spectra of the more luminous (solid line) and less luminous (dashed line) halves of the *IUE* sample.

To assess the Baldwin effect at low redshifts, the *IUE* sample was divided in half by luminosity, the split being made at an absolute magnitude of  $-24.8$ . Each half was separately co-added, and the analysis carried out as above. The two composites are shown in Fig. 7, and the Baldwin index is plotted in Fig. 8. Unfortunately, the more luminous QSOs in the *IUE* sample are at higher redshifts than the less luminous ones, and the bright subsample also has a high proportion of radio-loud QSOs.

Both composites show C IV Baldwin effects with roughly equal sizes, and in both the Baldwin effect is  $\sim 3$  times

stronger in the red wing of C IV than in the blue wing. Our mean C IV Baldwin index ( $\sim 0.15$ ) is well within the spread of measurements reported by other authors (e.g. the compilation in Francis et al. 1992), and close to the result of Zamorani et al. (1992) for complete samples of QSOs with comparable luminosities.

Could the excess Baldwin effect in the red wing of C IV be due to systematic redshift errors between the samples? The LBQS and Boyle samples had different redshift determination methods, but the lack of a strong Baldwin effect to the red of Ly $\alpha$  argues against such an effect. Redshifts were

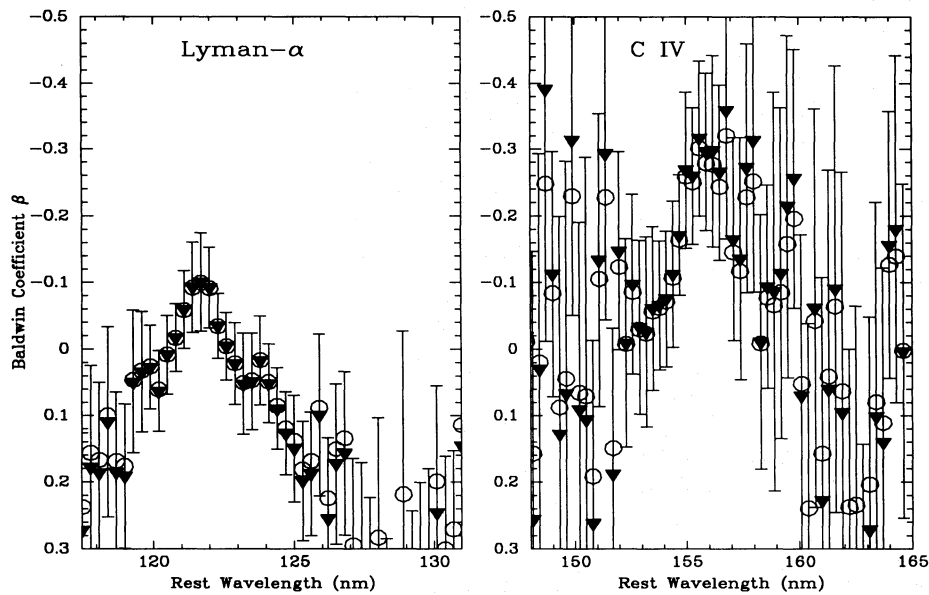


**Figure 8.** Wavelength dependence of the Baldwin effect, from the comparison of the more and less luminous *IUE* composite spectra. Solid triangles and error bars are derived from a best ‘by eye’ power-law continuum fit, while circles are derived from a different continuum fit, as described in the text.

determined for both halves of the *IUE* sample in the same way, so no bias is likely.

In both the high- and low-redshift comparisons, a smaller Baldwin effect is seen in  $\text{Ly}\alpha$  than in  $\text{C IV}$ , as reported by many authors. However, the  $\text{Ly}\alpha$  Baldwin effect appears stronger in the *IUE* sample. This may reflect evolution, but the different redshift ranges and radio properties of the two *IUE* subsamples may also be significant.

### 3.2 Profile-fitting

We have seen that the mean spectral properties of the *IUE* and LBQS samples are different, but the composite spectra cannot tell us if the evolution is due to small differences in all QSOs or to the emergence of some new subpopulation of QSOs at high or low redshift. For this, we need to measure the spectral properties of individual QSOs.

#### 3.2.1 The model

The measurement of QSO spectra is infamously subjective, due to the absence of unblended emission lines and the lack of good continuum windows (Francis et al. 1991); an enormous number of approaches have been used. We experimented with the  $\chi^2$  fitting of a wide variety of line and continuum models to the spectra. Models with many free parameters gave good fits, but were unacceptably sensitive to signal-to-noise ratio variations. In particular, models in which linewidths and/or the redshift displacements between different emission lines were allowed as free parameters behaved unacceptably in the noisier spectra, with the lines typically fitting themselves to narrow noise features.

Our adopted model is based on the deconvolution of the UV spectra into independent components proposed by Francis et al. (1992) and Wills et al. (1993b). They claim that

most UV spectral lines can be modelled by two largely independent components, a narrow line-core component called the Intermediate Line Region (ILR) and a much broader line-wing component called the Very Broad-Line Region (VBLR).

The continuum is modelled as a power law.  $\text{N v}$  (124.0 nm), the  $\text{Si IV/O IV}$  blend (140.0 nm) and the broad wings of  $\text{Ly}\alpha$  and  $\text{C IV}$  are all modelled as Gaussians whose peak heights are free parameters, but with fixed velocity widths of  $9000 \text{ km s}^{-1}$  (FWHM). The cores of  $\text{Ly}\alpha$  and  $\text{C IV}$  are modelled by Gaussians of fixed width  $2800 \text{ km s}^{-1}$ . The broad component of  $\text{C IV}$  was centred  $200 \text{ km s}^{-1}$  to the blue of its nominal wavelength, which slightly improved the fit, all other line components being at their nominal wavelengths. As a final, ninth free parameter, all fluxes shortward of the peak of  $\text{Ly}\alpha$  were multiplied by a constant factor, to allow for the integrated effect of  $\text{Ly}\alpha$ -forest absorption.

The fits of this model look respectable, and it gives sensible answers for even the poorest quality spectra. We do not, however, pretend that this model is a formally successful fit to the data. However, the continuum slopes, line-core strengths, line-wing strengths, line ratios and  $\text{Ly}\alpha$  decrements measured by this method agree well with those obtained from PCA (Section 3.3), with those obtained interactively using standard IRAF routines, and with the formally adequate model fits of the better quality spectra obtained by Francis et al. (1995, in preparation).

#### 3.2.2 Mean properties

The average line parameters and standard deviations for the *IUE* and LBQS samples are shown in Table 1. Standard deviations quoted are those of the sample, not of the mean. Peak heights are the height of the centre of the Gaussian above the continuum and should be multiplied by the line-

**Table 1.** Average emission-line peak heights.

Line	Line Peak Height	
	IUE	LBQS
QSO number	39	206
Lyman- $\alpha$ Core	$1.73 \pm 1.22$	$0.79 \pm 1.28$
Lyman- $\alpha$ Wings	$1.42 \pm 0.42$	$1.17 \pm 0.46$
N V	$0.49 \pm 0.42$	$0.65 \pm 0.20$
140 nm Blend	$0.16 \pm 0.17$	$0.15 \pm 0.09$
C IV Core	$0.39 \pm 0.46$	$0.20 \pm 0.35$
C IV Wings	$0.55 \pm 0.34$	$0.41 \pm 0.17$

**Table 2.** Peak heights of N v.

Sub-sample		N(QSO)	Line Peak height
IUE	Radio-loud	23	$0.40 \pm 0.23$
	Radio-quiet	15	$0.59 \pm 0.25$
LBQS	Radio-loud	7	$0.53 \pm 0.07$
	Radio-quiet	199	$0.67 \pm 0.19$

widths (Section 3.2.1) to get relative fluxes. All spectra were redshifted and normalized as described in Section 3.1 before the fitting.

The biggest differences between the samples are seen in the cores of Ly $\alpha$  and C IV, both of which are roughly a factor of 2 stronger in the IUE sample than in the LBQS sample. Both differences are significant at better than the  $2\sigma$  level. The wings of both lines are also stronger in the IUE sample, but by a much smaller amount, and with lower significance. This confirms the result of Section 3.1 above that the bulk of

the evolution is in the cores of Ly $\alpha$  and C IV. No evolution is seen in the 140.0-nm blend, but N v changes in the opposite sense, being stronger in the LBQS sample.

To see if the different radio-loud fractions in the IUE and LBQS samples could be responsible for the difference in the mean strength of N v, we averaged its strength separately for the radio-loud and radio-quiet QSOs of both samples. The results are shown in Table 2; errors are the standard deviations of the samples and not of the means. In both samples, N v is stronger in the radio-quiet QSOs. The significance of this difference was calculated using the Kolmogorov-Smirnov (KS) test; the difference was significant at the 2.1 per cent level in the IUE sample, and at the 3.4 per cent level in the LBQS sample. For subsamples with the same radio properties, N v is weaker in the IUE sample; however, these differences are of marginal significance (11 per cent for the radio-loud QSOs and 69 per cent for the radio-quiet QSOs). Note that this possible evolution in the strength of N v emission is consistent with the claim by Hamann & Ferland (1992) that the strength of N v emission increases with redshift.

### 3.2.3 Distributions

The distribution of Ly $\alpha$  and C IV line-core equivalent widths as a function of redshift are shown in Figs 9 and 10. The difference between the samples is immediately obvious; while both distributions have similar shapes at high equivalent widths, the LBQS has large numbers of weak line-core QSOs not seen in the IUE sample. The two distributions are histogrammed in Fig. 11. The IUE distribution is roughly Gaussian, with a standard deviation of  $\sim 30$  per cent of its mean value, while for the LBQS, the mode of the distribution is at zero, and the distribution can be approximated by an exponential.

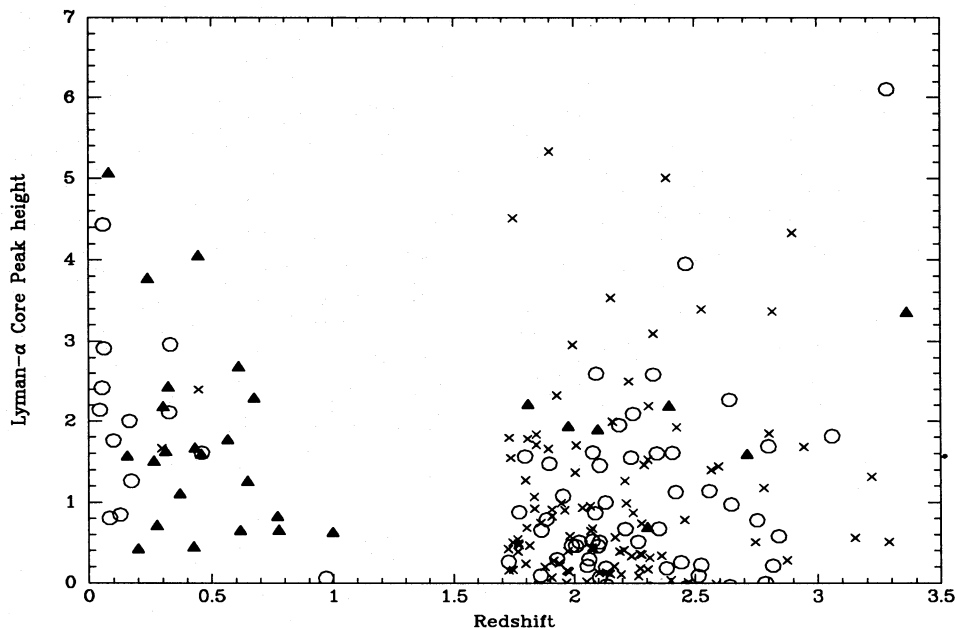


**Figure 9.** The distribution of Ly $\alpha$  line-core peak strengths (measured from the model fitting) as a function of redshift. Radio-loud QSOs are shown as solid triangles, radio-quiet as circles, and QSOs of unknown radio properties as crosses.

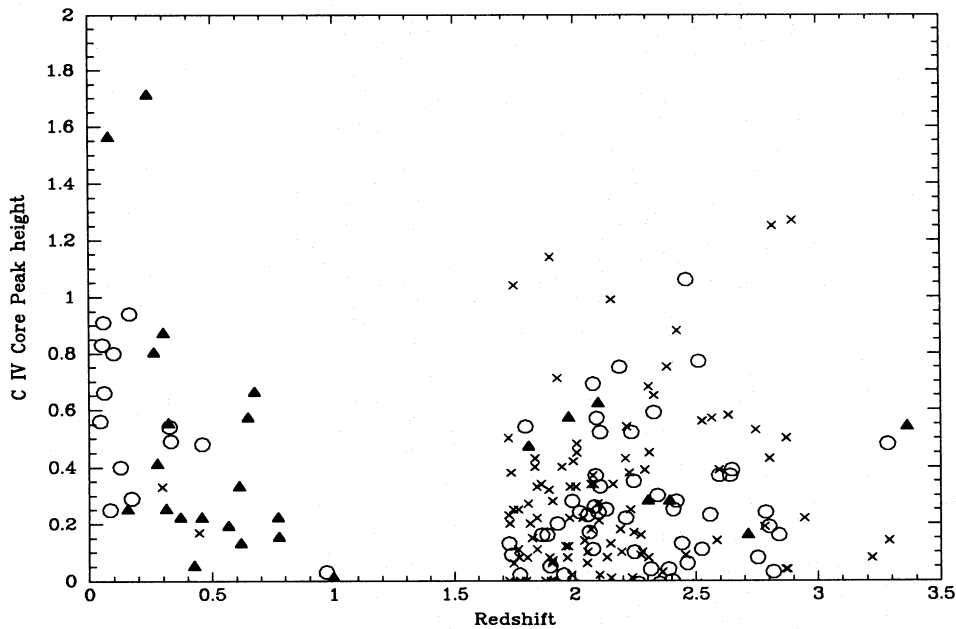


**Figure 10.** The distribution of C IV line-core peak strengths (measured from the model fitting) as a function of redshift. Radio-loud QSOs are shown as solid triangles, radio-quiet as circles, and QSOs of unknown radio properties as crosses.

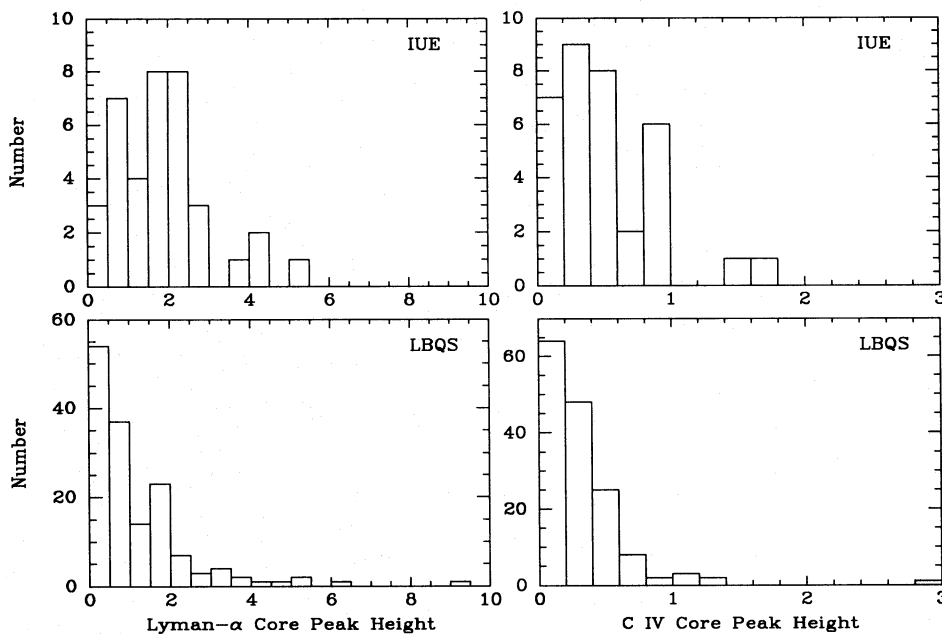


**Figure 11.** Histograms of the distributions of line-core peak strengths. Ly $\alpha$  is shown in the left panels, C IV in the right. The top panels show the *IUE* sample, and the *LBQS* is shown in the bottom panels.

The KS-test significance of the difference in Ly $\alpha$  line-core strengths between the *LBQS* and *IUE* samples is  $1.5 \times 10^{-5}$ , while for C IV the significance is  $4.7 \times 10^{-3}$ .

If a substantial fraction of the *IUE* QSOs were deliberately chosen to have strong and/or narrow emission lines, this might account for the difference. Prior to these *IUE* spectra, however, the UV line strengths of these objects were unknown. We would therefore require that the QSOs be selected on some property of their optical spectra that correlates strongly with the strength of the UV line cores.

Furthermore, the bias would have to be strong; to bring the *IUE* Ly $\alpha$  line-core strength distribution into line with that of the *LBQS*,  $\sim 20$  new weak line-core spectra would have to be added. We therefore conclude that the difference is real and unlikely to be a selection effect.

### 3.3 Multivariate analysis

To separate out the dependences of the emission-line core strengths on redshift, luminosity and radio emission, we use

non-parametric multivariate statistics. The procedure is as follows.

(i) A cosmology, defined by  $H_0$  and  $q_0$  is constructed, and absolute magnitudes are computed. The continuum slope  $\alpha$  ( $F_\nu \propto \nu^\alpha$ ) used to perform the  $k$ -corrections is also a free parameter.

(ii) A Baldwin coefficient  $\beta$  is chosen ( $W \propto L^\beta$ ).

(iii) The line-core strength for each QSO is corrected, using the Baldwin coefficient, to what its value would be if the QSO had an absolute magnitude of  $-25$ . As the line-core strengths  $W$  are measured from normalized spectra, they are effectively equivalent widths.

(iv) For the *IUE* and LBQS samples separately, Spearman's rank test is applied to the corrected line-core strengths. This evaluates the probability that the corrected data do not correlate with luminosity, and hence high probabilities indicate that an appropriate value of  $\beta$  was chosen.

(v) The line-core strength distributions (after correction) of the *IUE* and LBQS samples are compared, using the KS test. This yields the probability that the two samples are drawn from the same parent population; i.e. that no evolution is needed.

(vi) Finally, the probabilities obtained (that  $\beta$  is appropriate to the *IUE* sample, to the LBQS sample, and that for this value of  $\beta$  no evolution is necessary) are multiplied together to give the joint probability that a no-evolution model with this particular value of the Baldwin coefficient  $\beta$  fits the data.

This is repeated for a range of values of the Baldwin coefficient  $\beta$ . The assumed value of  $\beta$  is applied to the equivalent widths of the whole measured component, i.e. the

line cores. Results are shown in Figs 12 and 13, for  $H_0 = 75$  km s $^{-1}$  Mpc $^{-1}$ ,  $q_0 = 0.5$  and  $\alpha = -0.3$ . A wide range of cosmological parameters and  $k$ -correction slopes were used, and the conclusions were insensitive to them. We will discuss the results for Ly $\alpha$  using the line-core strengths derived from Section 3.2 (Fig. 12); the results for C IV (Fig. 13) are similar, but the constraints weaker. The analysis can be repeated using the first component weight from the PCA analysis (below); the results are almost identical to those obtained from Ly $\alpha$ .

For the *IUE* sample,  $\beta \sim -0.2$  is a good fit both for the radio-loud and radio-quiet populations, but quite a wide range of values are possible at the 10 per cent level:  $\beta < 0$  for the radio-quiet QSOs and  $\beta > -0.5$  for the radio-loud. For the LBQS, weaker ( $\beta$  more positive) Baldwin effects give better fits but, once again, at the 10 per cent level a wide range of values are acceptable. For the radio-loud QSOs, a small positive value of  $\beta$  eliminates evolutionary differences between the *IUE* and LBQS samples; for the radio-quiet QSOs, no value of  $\beta$  does a very good job of removing evolution, but for  $\beta < -0.3$  a fit acceptable at the 30 per cent level can be obtained.

The joint probabilities show that the radio-loud population can be fitted by the no-evolution model at about the 15 per cent confidence level. This requires  $\beta \sim 0.1$ ; i.e. the line equivalent width weakly *correlates* with luminosity, the opposite of the normal Baldwin effect. However, the constraints are not tight, and  $\beta \sim -0.15$ , as found in the literature and measured in Section 3.1.3, is acceptable at the 1 per cent level.

For the radio-quiet QSOs, no value of  $\beta$  gives an acceptable fit. The peak joint probability is less than 1 per cent,

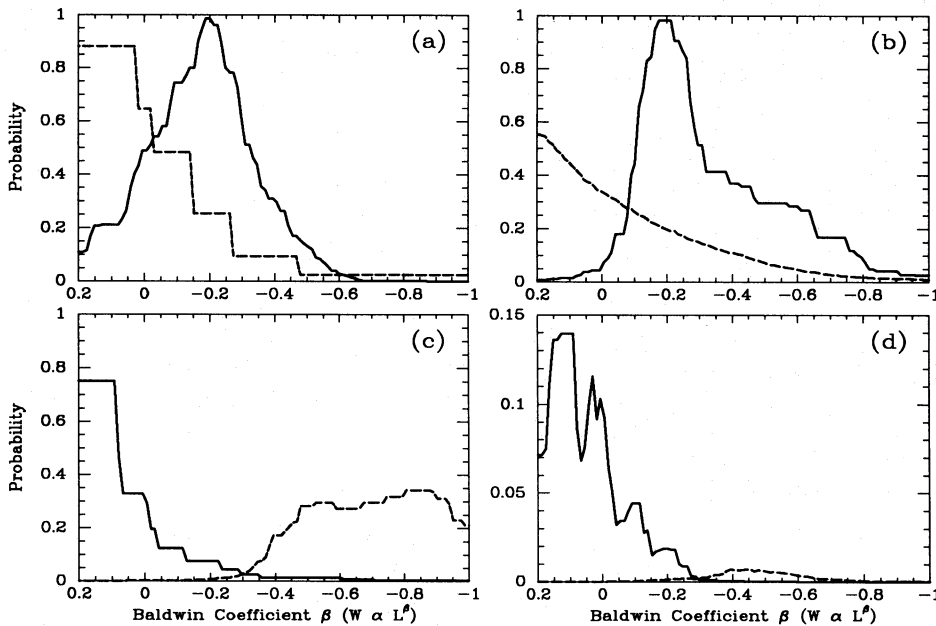


**Figure 12.** The goodness-of-fit of the Baldwin effect model to the cores of the Ly $\alpha$  emission line. (a) shows the probability that after correction by a Baldwin effect of index  $\beta$ , the line-core equivalent widths are uncorrelated with luminosity, as a function of  $\beta$ . The solid line is for radio-loud *IUE* QSOs, the dashed line for radio-loud LBQS QSOs. (b) is the same as (a), but for radio-quiet QSOs. (c) shows the probability that after correction for the Baldwin effect, there is no significant difference between the *IUE* and LBQS samples (solid line for radio-loud, dashed line for radio-quiet). (d) shows the joint probabilities of getting these data assuming the null hypothesis (no evolution) as a function of  $\beta$  (solid line for radio-loud, dashed line for radio-quiet).

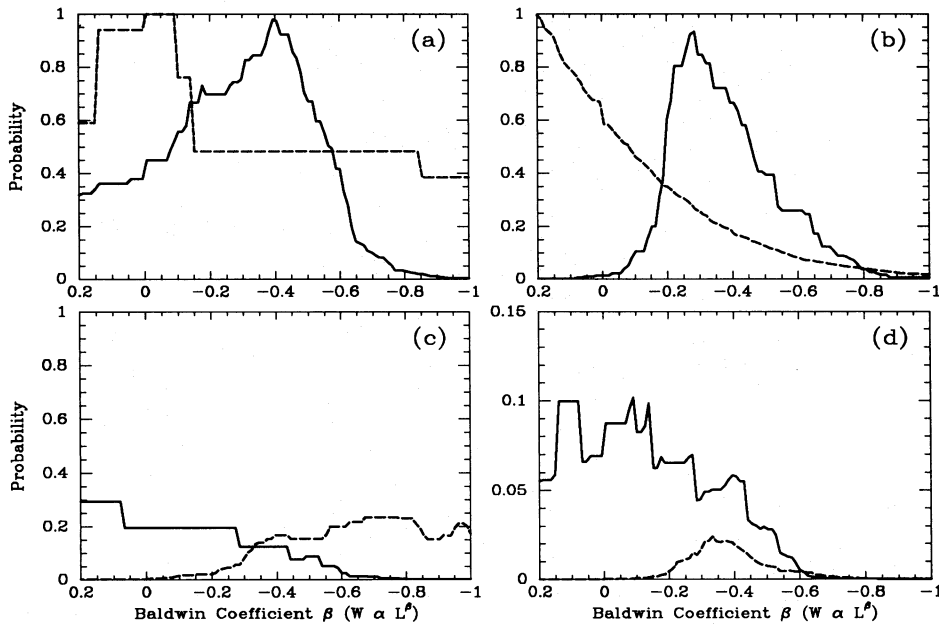


Figure 13. As Fig. 12, but for C IV.

occurring at  $\beta \sim -0.4$ , a substantially higher value of  $\beta$  than that found in Section 3.1.3. Why is this? The best-fitting Baldwin effects are weak ( $\beta \sim -0.2$ ), but to eliminate evolution a much stronger Baldwin effect is needed ( $\beta \sim -0.6$ ). The reason is that the distributions of line-core strengths in the two samples are different; the LBQS has a population of QSOs with weak line cores not seen in the *IUE* sample. If we choose an overstrong Baldwin effect, the line-core strengths of the brightest QSOs are corrected down to small values, giving the *IUE* sample a population of weak line-core QSOs.

We therefore conclude that evolution is required to explain the data. The null hypothesis (no evolution) can be rejected with 99 per cent confidence for the radio-quiet QSOs, but with only 86 per cent confidence for the radio-loud QSOs. However, if we require the radio-loud QSOs to have the same Baldwin coefficient as measured by the composite comparison and by other authors, the null hypothesis can be rejected with 98 per cent confidence.

### 3.4 Principal Components Analysis (PCA)

The technique of Principal Components Analysis (PCA), as presented by Francis et al. (1992), has two major advantages over more conventional spectral analysis techniques. It is model-independent and, crucially for this present work, it is extremely robust in handling spectra with poor signal-to-noise ratios. Indeed, it can be formally shown to be the optimal linear least-squares method of measuring spectral parameters. We apply it, using the method of Francis et al. (1992) and FHI, to our combined sample of *IUE* and LBQS spectra.

The two largest principal components are very similar to those obtained by Francis et al. The first is dominated by the line-core emission in Ly $\alpha$  and C IV. Note that, using PCA, the contributions of C IV and Ly $\alpha$  cannot be separated out; the

first component weight is equivalent to their weighted sum. The second principal component is dominated by the continuum slopes, and shows no correlations with redshift or luminosity. The third principal component is dominated by the wings of the broad emission lines, and hence is similar to the fourth component of Francis et al. The third (broad-absorption-line) component of Francis et al. is absent, as would be expected due to the exclusion of broad-absorption-line QSOs from the LBQS and *IUE* samples.

The fourth principal component is not seen in the Francis et al. study. It is dominated by a depression running from the blue end of the spectra to the peak of Ly $\alpha$ , suggesting that it is caused by Ly $\alpha$ -forest absorption. Indeed, its strength correlates tightly with redshift, the slope of the correlation being consistent with published measurements of the evolution in the Ly $\alpha$  forest, and it also correlates strongly with the Ly $\alpha$  decrement parameter described above.

The mean weights of each of the first three components in the two samples are listed in Table 3. Errors in the component weights are the standard deviations of the sample, not of the mean, but the errors in the difference column are for the means.

Table 3 shows that the second (continuum-slope) and third (line-wing) components do not significantly differ between the *IUE* and LBQS samples. The lack of a dif-

Table 3. Weights of the principal components.

Component	<i>IUE</i> Weight	LBQS weight	Difference
QSO number	39	206	
1	$-1.80 \pm 2.10$	$0.34 \pm 2.41$	$-2.14 \pm 0.38$
2	$0.11 \pm 1.54$	$-0.02 \pm 0.90$	$0.13 \pm 0.25$
3	$-0.10 \pm 0.98$	$0.02 \pm 0.60$	$0.11 \pm 0.16$

ference in the line wings contradicts the marginal result found in Section 3.2; the discrepancy is not significant, and may be due to some part of the line-core influencing the line-wing fits. A difference is seen in the first component weights, which are more negative in the *IUE* sample. This reflects the stronger line cores in C IV and Ly $\alpha$  in the *IUE* sample.

The distribution of first-component weights as a function of redshift is very similar to Figs 9 and 10; a population of QSOs with weak line cores is seen in the LBQS sample but not in the *IUE* sample. A KS test comparing the first-component weights of the *IUE* and LBQS samples rates the difference as significant at the  $2.4 \times 10^{-6}$  level.

The PCA analysis thus confirms the results of the model-fitting analysis.

## 4 DISCUSSION

We have shown that the cores of Ly $\alpha$  and C IV evolve between redshift  $z \sim 2$  and the present; at low redshifts, both radio-loud and radio-quiet QSOs have similar distributions of line-core strengths, whereas at  $z \sim 2$ , radio-quiet QSOs have a distribution of line-core strengths which peaks at small values. This paper thus joins a growing series which identify the line cores as interesting features.

(i) Francis et al. (1992) used PCA to show that the cores of the emission lines Ly $\alpha$  and C IV vary independently of the rest of the spectrum, and account for the bulk of the diversity of the QSO population. This was independently confirmed by Wills et al. (1993b).

(ii) FHI showed that at high redshifts ( $z \sim 2$ ) the difference between the spectra of radio-loud and radio-quiet spectra was in the cores of the emission lines, the cores being stronger in radio-loud QSOs. This was independently confirmed by Brotherton et al. (1994a).

(iii) Osmer et al. (1994) claim that the Baldwin effect is dominated by the line cores, as tentatively suggested by Francis et al. (1992). Their results, however, differ in detail from those in Section 3.1.3, and lack formal errors.

(iv) Brotherton et al. (1994b) separated out the spectra of the line cores and the line wings, and modelled the line cores as emission from an ILR, with properties intermediate between those of the classical broad-line and narrow-line regions.

In this section, we ask why at high redshift a large fraction of radio-quiet QSOs should have weak line-core emission.

### 4.1 Gravitational microlensing

If a QSO is lensed by a galaxy or cluster of galaxies, its spectrum will be unaffected by the lensing, as the equivalence principle ensures that light at all wavelengths is lensed equally. If the lensing object is much smaller, however, it may only lens part of the QSO, and thus change the relative prominence of that part in the observed spectrum. QSOs at  $z \sim 2$  are most strongly lensed by objects at redshifts  $0.5 < z < 1$ , and these lenses will strongly amplify sources with angular sizes comparable to the Einstein radii of the lensing objects,  $\sim 10^{-6} \sqrt{M/M_{\odot}}$  arcsec.

Models of the emission-line region of QSOs (Brotherton et al. 1994b) suggest that the line-core emission comes from regions  $\sim 0.5$  pc from the central engine and the line-wing

emission from scales  $\sim 0.05$  pc. The continuum radiation will come from smaller regions still. Thus compact objects at  $z \sim 0.8$  with masses  $\sim 1 M_{\odot}$  would be capable of lensing the line-wing emission without lensing the line-core emission appreciably. The separation of images from a lens such as this will be of order microarcsec and hence quite unobservable; the amplification of the line-wing flux will, however, be measurable.

Thus if microlensing by solar mass compact objects was important it would amplify the continuum and line-wing emission of high-redshift QSOs, without affecting their line-core emission. High-redshift samples would therefore include a population of QSOs with low equivalent-width line cores, the heavily microlensed QSOs. This could thus potentially explain the evolution measured in this paper.

Microlensing has been detected in at least one QSO (Corrigan et al. 1991). It has been invoked to explain the variability of QSOs (Hawkins 1993), and the observed excess of QSOs around foreground galaxies (Rodrigues-Williams & Hogan 1994). How much is needed to explain the evolution of line-core strengths?

Canizares (1982) and Delcanton et al. (1994) have modelled this microlensing effect, and find that if about 5 per cent of the critical density of the Universe is made up of compact objects, many bright QSOs at  $z > 1$  will be microlensed. If we take the *IUE* sample, put it at  $z \sim 1$ , and microlens it with solar-mass compact objects, uniformly distributed and contributing 5 per cent of the critical density, then using the models of Delcanton et al., we find that its line-core equivalent-width distribution would closely resemble that of the LBQS. Thus microlensing can, in principle, explain the observed evolution. Note that the limits Delcanton et al. place on the density of brown-dwarf-mass objects are not relaxed; such objects would cause evolution in the equivalent widths of the line wings, which we do not observe. We require larger lensing masses.

Why is evolution not seen in the radio-loud QSOs? The radio-loud LBQS QSOs were optically selected, and hence are subject to the same amplification bias as the rest of the sample. The radio emission probably comes from too large a region to be microlensed, so lensed QSOs will have lower radio-to-optical ratios than unlensed ones; for typical lensing amplitudes of  $\sim 3$ , this effect is not, however, sufficient to cause many QSOs to be misclassified as radio-quiet (FHI). We therefore conclude that the lack of evolution in the radio-loud QSOs is an argument against microlensing.

The microlensing picture is elegant, and can explain the evolution in the spectra of radio-quiet QSOs well. However, a very large density of solar-mass compact objects is required, and the lack of evolution in radio-loud QSOs is hard to explain. If the strength of N V emission does evolve, this would also be inexplicable in the microlensing model.

### 4.2 Orientation effects

It is currently popular to ascribe many differences between the spectra of QSOs to the angle of viewing. If both samples were randomly oriented, this could not cause evolution in the spectra. However, if the continuum emission of QSOs is anisotropic, both samples will be biased toward those QSOs beaming their light in our direction. The steeper the luminosity function, the stronger the bias will be.

Hewett et al. (1993) showed that for luminous QSOs, the luminosity function is steeper at high redshifts. A high-redshift sample will thus be biased towards beamed QSOs. Assuming the continuum radiation to be emitted less isotropically than the line radiation, this implies that high-redshift QSOs will have lower emission-line equivalent widths.

The effect of orientation upon QSO spectra has been modelled by Francis (1993a). Using this formalism, combined with the luminosity functions of Hewett et al. (1993), we can calculate the expected evolution in emission-line equivalent widths, if we assume a particular continuum source anisotropy. For a thin accretion disc continuum source, orientation effects will reduce the equivalent widths of the high-redshift sample by 17 per cent, roughly half the observed evolution. The change in the equivalent width distribution does not, however, match the observations; this model predicts that the change comes from a new population of very high equivalent-width QSOs at low redshifts, not a new population of very low equivalent-width QSOs at high redshift.

We therefore conclude that orientation effects cannot explain the observed evolution.

### 4.3 Dust

Webster et al. (1995) have recently claimed that most radio-loud quasars are obscured by some quantity of dust along the line of sight to their central engine. The location of the dust is unknown, but in some cases it seems to obscure the broad-line region but not the narrow-line region, leading to abnormally high forbidden-line equivalent widths.

If dust is also found in radio-quiet QSOs, it may explain some of the spectral evolution reported in this paper. Even a small quantity of dust will dramatically reduce the observed *B*-band flux of a high-redshift QSO, causing it to drop below the magnitude limit of a sample such as the LBQS. Thus the LBQS sample is strongly biased against dust-obscured QSOs, while the *IUE* sample may be less so, being selected either in the radio or at longer (and hence less dust-affected) rest-frame wavelengths.

If, furthermore, the dust is clumpy on scales comparable to the size of the broad-line region, it will sometimes obscure the continuum emitting and line-wing emitting regions of a QSO, but not the larger line-core emitting regions. These partially obscured QSOs will show abnormally high line-core equivalent widths. Thus the more biased a sample is against dust-obscured QSOs, the higher its line-core equivalent widths. The LBQS, being more strongly biased, would thus have the high line-core equivalent widths, as observed.

This model has two problems. First, it is not clear that the *IUE* sample will be any less biased against dust-obscured QSOs than the LBQS. While the original selection will not be as strongly dust-affected as for the LBQS, only QSOs which are very bright in the UV have good-quality *IUE* spectra and hence can be included in our sample.

Secondly, this model cannot explain the differences between the evolution of radio-loud and radio-quiet spectra, unless radio-quiet QSOs are on average obscured by more dust than radio-loud. In principle, dust could cause radio-quiet QSOs to be misclassified as radio-loud, by absorbing the optical flux and hence boosting the radio-to-optical

ratios. However, radio-loud and radio-quiet QSOs are separated by a factor of roughly 100 in radio-to-optical ratio (FHI), so a dust extinction of 5 mag in the optical would be required to make an intrinsically radio-quiet QSO appear radio-loud. This amount of dust would put almost any QSO below the magnitude cut-off of a sample such as the LBQS.

We conclude that while biases against dust-obscured QSOs may be important in our samples, they are unlikely to be responsible for the observed spectral evolution.

### 4.4 Intrinsic evolution

If spectral evolution is intrinsic to the QSOs, the fact that it is seen only in the low-velocity cores of the emission lines is an important clue. If the evolution was due to a change in the ionizing flux, or to some flow of gas from the nucleus, it would probably affect the inner high-velocity gas as well as the more distant line-core gas.

This suggests that the evolution is caused by the QSO environment and not the QSO central engine. Somehow, the environments of high-redshift radio-quiet QSOs inhibit the formation of extensive line-core emitting regions.

A possible clue to the nature of this effect comes from the narrow-line region. Narrow emission lines, such as [O II] (372.7 nm) and [O III] (500.7 nm) are substantially stronger in radio-loud than in radio-quiet QSOs, and have roughly exponential equivalent-width distributions (Boroson & Green 1992). Thus the line cores of high-redshift QSOs behave like the narrow lines of low-redshift QSOs. The low-redshift behaviour of the line cores (no difference between radio-loud and radio-quiet QSOs, Gaussian equivalent-width distributions) is more typical of the wings of the broad lines.

Thus at  $z \sim 2$  the statistical behaviour of the outer broad-line region is similar to that of the narrow-line region, but at low redshift it is similar to that of the inner broad-line region. The boundary between the two types of statistical behaviour is moving inward.

Given our ignorance of the nature of the emission-line regions, this tells us little about the physics of QSO evolution, but it does suggest that the hitherto separate problems of QSO evolution, radio-loudness and the nature of the emission-line regions are closely related, and that an understanding of the difference between the broad- and narrow-line regions may be of crucial importance.

## 5 CONCLUSIONS

We have compared the UV spectra of high- and low-redshift QSOs and we find the following.

- (i) The UV spectra of radio-quiet QSOs evolve between  $z \sim 2$  and the present.
- (ii) At high redshift, many radio-quiet QSOs have weak emission-line cores. The weak cores are probably caused by unusually compact broad emission-line regions.
- (iii) No significant evolution is seen in the spectra of radio-loud quasars.
- (iv) N v emission is weak in radio-loud QSOs.
- (v) The Baldwin effect is stronger in the red wing of C IV than in the blue wing.

**ACKNOWLEDGMENTS**

We thank Mike Corbin, Pat Osmer, Rachel Webster and Bev Wills for many fruitful discussions, and Stuart Williams for making interactive measurements of line parameters. The LBQS is supported by National Science Foundation grant AST 90-01181, for which we are grateful. We also thank Brian Boyle for making a digital copy of his composite spectrum available to us. PJF is supported by an ARC grant.

**REFERENCES**

- Bohlin R. C., Grillmair C. J., 1988, *ApJS*, 66, 209  
 Bohlin R. C., Harris A. W., Holm A. V., Gry C., 1990, *ApJS*, 73, 413  
 Boroson T. A., Green R. F., 1992, *ApJS*, 80, 109  
 Boyle B. J., 1990, *MNRAS*, 243, 231  
 Brotherton M. S., Wills B. J., Steidel C. C., Sargent W. L. W., 1994a, *ApJ*, 423, 131  
 Brotherton M. S., Wills B. J., Francis P. J., Steidel C. C., 1994b, *ApJ*, 430, 495  
 Canizares C. R., 1982, *ApJ*, 263, 508  
 Chaffee F. H., Foltz C. B., Hewett P. C., Francis P. J., Weymann S. L., Morris S. L., Anderson S. F., MacAlpine G. M., 1991, *AJ*, 102, 461  
 Corrigan R. T. et al., 1991, *AJ*, 102, 34  
 Delcanton J. J., Canizares C. R., Granados A., Steidel C. C., Stocke J. T., 1994, *ApJ*, 424, 550  
 Durret F., 1989, *A&AS*, 81, 253  
 Foltz C. B., Chaffee F. H., Hewett P. C., MacAlpine G. M., Turnshek D. A., Weymann R. J., Anderson S. F., 1987, *AJ*, 94, 1423  
 Foltz C. B., Chaffee F. H., Hewett P. C., Weymann R. J., Anderson S. F., MacAlpine G. M., 1989, *AJ*, 98, 1959  
 Francis P. J., 1993a, *ApJ*, 405, 119  
 Francis P. J., 1993b, *ApJ*, 407, 519  
 Francis P. J., Hewett P. C., Foltz C. B., Chaffee F. H., Weymann R. J., Morris S. L., 1991, *ApJ*, 373, 465  
 Francis P. J., Hewett P. C., Foltz C. B., Chaffee F. H., 1992, *ApJ*, 398, 476  
 Francis P. J., Hooper E. J., Impey C. D., 1993, *AJ*, 106, 417 (FHI)  
 Haehnelt M. G., Rees M. J., 1993, *MNRAS*, 263, 168  
 Hamann F., Ferland G., 1992, *ApJ*, 391, L53  
 Hawkins M. R. S., 1993, *Nat*, 366, 242  
 Heckman T. M., Lehnert M. D., van Breugel W., Miley G. K., 1991, *ApJ*, 370, 78  
 Hewett P. C., Foltz C. B., Chaffee F. H., Francis P. J., Weymann R. J., Morris S. L., Anderson S. F., MacAlpine G. M., 1991, *AJ*, 101, 1121  
 Hewett P. C., Foltz C. B., Chaffee F. H., 1993, *ApJ*, 406, L43  
 Hu E., Songaila A., Cowie L., Stockton A., 1991, *ApJ*, 368, 28  
 Junkkarinen V., Hewitt A., Burbidge G., 1991, *ApJS*, 77, 263  
 Kellerman K., Sramek R., Schmidt M., Shaffer D., Green R., 1989, *AJ*, 98, 1195  
 Kinney A. L., Bohlin R. C., Neill J. D., 1991, *PASP*, 103, 694  
 Morris S. L., Weymann R. J., Anderson S. F., Hewett P. C., Foltz C. B., Chaffee F. H., Francis P. J., MacAlpine G. M., 1991, *AJ*, 102, 1627  
 Neugebauer G., Green R. F., Matthews K., Schmidt M., Soifer B. T., Bennett J., 1987, *ApJS*, 63, 615  
 Osmer P. S., Porter A. C., Green R. F., 1994, *ApJ*, 436, 678  
 Rodrigues-Williams L. L., Hogan C. J., 1994, *AJ*, 107, 451  
 Schmidt M., Green R. F., 1983, *ApJ*, 269, 352  
 Small T. A., Blandford R. D., 1992, *MNRAS*, 259, 725  
 Stockton A., MacKenty J., 1987, *ApJ*, 316, 584  
 Véron-Cetty M.-P., Véron P., 1989, *ESO Scientific Report*, No. 7  
 Visnovsky K. L., Impey C. D., Foltz C. B., Hewett P. C., Weymann R. J., Morris S. L., 1992, *ApJ*, 391, 560  
 Webster R. L., Francis P. J., Peterson B. A., Drinkwater M. J., Masci F. J., 1995, *Nat*, submitted  
 Wills B. J., Netzer H., Brotherton M. S., Han M., Wills D., Baldwin J. A., Ferland G. J., Browne I. W. A., 1993a, *ApJ*, 410, 534  
 Wills B. J., Brotherton M. S., Fang D., Steidel C. C., Sargent W. L. W., 1993b, *ApJ*, 415, 563  
 Zamorani G., Marano B., Mignoli M., Zitelli V., Boyle B. J., 1992, *MNRAS*, 256, 238